

## Original Article

## Transcriptionally distinct malignant neuroblastoma populations show selective response to adavosertib treatment

Chiao-Hui Hsieh <sup>a,1</sup>, Yi-Xuan Chen <sup>a,1</sup>, Tzu-Yang Tseng <sup>a</sup>, Albert Li <sup>b</sup>, Hsuan-Cheng Huang <sup>c,\*</sup>, Hsueh-Fen Juan <sup>a,b,d,e,\*</sup>

<sup>a</sup> Department of Life Science, National Taiwan University, Taipei, Taiwan

<sup>b</sup> Graduate Institute of Biomedical Electronics and Bioinformatics, National Taiwan University, Taipei, Taiwan

<sup>c</sup> Institute of Biomedical Informatics, National Yang Ming Chiao Tung University, Taipei, Taiwan

<sup>d</sup> Center for Computational and Systems Biology, National Taiwan University, Taipei, Taiwan

<sup>e</sup> Center for Advanced Computing and Imaging in Biomedicine, Taipei, Taiwan

## ARTICLE INFO

## Keywords:

Neuroblastoma  
Single cell RNA sequencing  
Adavosertib  
AKT/mTOR pathway  
Cancer therapy

## ABSTRACT

Neuroblastoma is an aggressive childhood cancer that arises from the sympathetic nervous system. Despite advances in treatment, high-risk neuroblastoma remains difficult to manage due to its heterogeneous nature and frequent development of drug resistance. Drug repurposing guided by single-cell analysis presents a promising strategy for identifying new therapeutic options. Here, we aim to characterize high-risk neuroblastoma subpopulations and identify effective repurposed drugs for targeted treatment. We performed single-cell transcriptomic analysis of neuroblastoma samples, integrating bulk RNA-seq data deconvolution with clinical outcomes to define distinct malignant cell states. Using a systematic drug repurposing pipeline, we identified and validated potential therapeutic agents targeting specific high-risk neuroblastoma subpopulations. Single-cell analysis revealed 17 transcriptionally distinct neuroblastoma subpopulations. Survival analysis identified a highly aggressive subpopulation characterized by elevated UBE2C/PTTG1 expression and poor patient outcomes, distinct from a less aggressive subpopulation with favorable prognosis. Drug repurposing screening identified Adavosertib as particularly effective against the aggressive subpopulation, validated using SK-N-DZ cells as a representative model. Mechanistically, Adavosertib suppressed cell proliferation through AKT/mTOR pathway disruption, induced G2/M phase cell cycle arrest, and promoted apoptosis. Further analysis revealed UBE2C and PTTG1 as key molecular drivers of drug resistance, where their overexpression enhanced proliferation, Adavosertib resistance, and cell migration. This study establishes a single-cell-based drug repurposing strategy for high-risk neuroblastoma treatment. Our approach successfully identified Adavosertib as a promising repurposed therapeutic agent for targeting specific high-risk neuroblastoma subpopulations, providing a framework for developing more effective personalized treatment strategies.

## Introduction

Neuroblastoma is the most common extracranial solid tumor in children and accounts for approximately 15% of all pediatric cancer-related deaths [1]. This malignancy arises from neural crest cells of the sympathetic nervous system and often presents with diverse symptoms

such as bone pain, abdominal distension, and fatigue [2,3]. Despite advances in surgical resection and cytotoxic chemotherapy, clinical outcomes for high-risk neuroblastoma remain poor, with a five-year survival rate of less than 50%. While current clinical treatments involve surgery and cytotoxic chemotherapy, the recent introduction of the International Neuroblastoma Risk Group (INRG)

**Abbreviations:** scRNA-seq, Single-cell RNA sequencing; INRG, International Neuroblastoma Risk Group; PARP, Poly (ADP-ribose) Polymerase; DEGs, Differentially expressed genes; PTTG1, Pituitary tumor transforming gene 1; UBE2C, Ubiquitin-conjugating enzyme (E2) family; GOSH, Great Ormond Street Hospital; PCA, Principal component analysis; GDSC, Genomics of Drug Sensitivity in Cancer; DMEM, Dulbecco's Modified Eagle Medium; FBS, Fetal bovine serum; RTCA, xCELLigence real-time cell analysis system; RT-qPCR, Quantitative real-time PCR; PVDF, Polyvinylidene difluoride; SD, Standard deviation; SEM, Standard error of mean.

\* Corresponding authors.

E-mail addresses: [hsuancheng@nycu.edu.tw](mailto:hsuancheng@nycu.edu.tw) (H.-C. Huang), [yukijuan@ntu.edu.tw](mailto:yukijuan@ntu.edu.tw) (H.-F. Juan).

<sup>1</sup> The authors contribute equally to this study.

<https://doi.org/10.1016/j.neurot.2025.e00575>

Received 12 November 2024; Accepted 8 March 2025

1878-7479/© 2025 The Author(s). Published by Elsevier Inc. on behalf of American Society for Experimental NeuroTherapeutics. This is an open access article under the CC BY-NC-ND license (<http://creativecommons.org/licenses/by-nc-nd/4.0/>).

classification system has allowed stratification of patients into distinct risk groups, yet the clinical management of high-risk neuroblastoma continues to face significant challenges, especially due to the disease's inherent heterogeneity [4–6]. One of the most critical obstacles in treating high-risk neuroblastoma is its pronounced intertumoral and intratumoral heterogeneity. This variability manifests as distinct molecular subtypes and cell populations within the tumor, leading to differential responses to therapy and the emergence of drug resistance [7,8]. Understanding the molecular basis of this heterogeneity is therefore essential for developing effective therapeutic strategies that can be tailored to the characteristics of each subpopulation.

The advent of single-cell RNA sequencing (scRNA-seq) has emerged as a transformative tool for unraveling the complexities of cellular heterogeneity in tumors [9]. This technology enables the identification of rare cell populations, reveals gene regulatory networks, and maps developmental trajectories, providing unprecedented insights into tumor biology [10–13]. In neuroblastoma, scRNA-seq has been employed to delineate cell states associated with therapy resistance and disease progression [14, 15]. Leveraging this capability, we sought to dissect neuroblastoma heterogeneity at a single-cell level, aiming to identify therapeutic vulnerabilities specific to the most malignant subpopulations.

In this study, we performed single-cell transcriptomic analysis of 6442 cells from the Neuroblastoma Cell Atlas to characterize distinct neuroblastoma subpopulations. We identified a highly aggressive subpopulation characterized by elevated UBE2C/PTTG1 expression that correlated with poor survival outcomes. To target this high-risk subpopulation, we integrated scRNA-seq data with drug response profiles from 14 neuroblastoma cell lines, leading to the identification of Adavosertib, a WEE1 kinase inhibitor, as a promising therapeutic candidate. Using SK-N-DZ cells as a representative model of the aggressive subpopulation, we demonstrated that Adavosertib effectively suppressed tumor growth by downregulating the AKT/mTOR pathway, inducing G2/M phase arrest, and promoting apoptosis. Mechanistic studies revealed that Adavosertib reduced the expression of UBE2C and PTTG1, genes critical to neuroblastoma pathogenesis and drug resistance. Together, these findings establish both UBE2C and PTTG1 as potential therapeutic targets and demonstrate how single-cell transcriptomics can guide drug repurposing strategies for personalized treatment of high-risk neuroblastoma.

## Materials and Methods

### Single-cell transcriptomic analysis and clustering of neuroblastoma samples

We utilized pre-processed single-cell transcriptomes from the Neuroblastoma Cell Atlas (<https://www.neuroblastomacellatlas.org/>), specifically analyzing five samples collected from Great Ormond Street Hospital (GOSH), comprising a total of 6442 cells [16]. For quality control, cells with a mitochondrial count exceeding 5% were excluded from further analysis. Log normalization was applied to correct for skewness in gene expression profiles. We then selected the top 2000 highly variable genes for dimensional reduction using principal component analysis (PCA), with the top 40 principal components employed for clustering. Cell clusters were identified through the Louvain algorithm and visualized using UMAP (Supplemental Figs. S1a, b, c, f) [17,18]. Manual annotation of cell clusters was conducted based on cell reference markers [16]. Differential gene expression analysis was performed to identify cluster-specific features, with pairwise comparisons between tumor clusters revealing three distinct sets of differentially expressed genes. All single-cell analyses were conducted using the Seurat package [19].

### Clustering analysis of bulk neuroblastoma cohorts using differential gene signatures

We analyzed two bulk neuroblastoma cohorts, TARGET and SEQC-NB498 dataset (GSE62564 and GSE49710), which include 127 and 498

patient samples, respectively [20,21]. Gene signature derived from the differentially expressed genes (DEGs) identified in the tumor clusters was used to classify the tumor cells. Clustering analysis was performed using Euclidean distance and complete linkage. Patients were divided into two subgroups based on the resulting dendrogram, and the gene expression patterns of these subgroups were thoroughly examined. The clustering was specifically carried out using Euclidean distance and complete linkage methods.

### Deconvolution of bulk RNA-seq data using CIBERSORTx based on single-cell reference profiles

CIBERSORTx was used to estimate the cell type proportions of bulk RNA-seq dataset using a reference gene expression profile [22]. We used six distinct identities, including endothelium, mesenchyme, leukocytes, and three tumor clusters (cluster 3, 9 and 13), from the single-cell data as the reference. The cell type composition of two neuroblastoma patient cohorts, TARGET and SEQC-NB498, was then deconvolved into six categories based on the single-cell reference profiles.

### Survival analysis using SEQC-NB498 dataset and Kaplan-Meier estimation

We used SEQC-NB498 dataset to reveal the relationship between genes and survival outcomes. Survival analysis was conducted using the R2 platform (<http://r2.amc.nl>). The Kaplan-Meier scanner was applied for each gene, with cutoff mode set as “scan” to determine the optimal expression threshold for distinguishing between cohorts with favorable and unfavorable prognoses. Both overall and event-free survival analyses were performed, and the results were visualized through survival curves.

### Drug discovery pipeline and correlation analysis for targeting malignant neuroblastoma

To identify drugs targeting malignant neuroblastoma clusters, we developed a drug discovery pipeline. After determining the signature genes of malignant cluster, we computed the signature score for each cell line by summing the expression levels of the signature genes. We then obtained drug response data from the Genomics of Drug Sensitivity in Cancer (GDSC) database and calculated the drug score based on IC<sub>50</sub> values and the area under drug response curve.

To assess drug efficacy, we employed a correlation analysis between the signature score and the drug score across multiple cell lines. This process allowed us to quantify the relationship between these two variables. We hypothesized that the strength of the correlation coefficient would indicate drug effectiveness, with a larger absolute value suggesting greater efficacy. The analytical framework allowed us to explore the relationship between signature genes and drug responses, offering valuable insights into drug efficacy and potential repurposing opportunities.

### Cell culture conditions for the neuroblastoma cell line

The human neuroblastoma cell line SK-N-DZ (CRL-2149) was used for the study. All cells tested negative for mycoplasma and were maintained in Dulbecco's Modified Eagle Medium (DMEM; Thermo Scientific, MA, USA) supplemented with 10% fetal bovine serum (FBS; Thermo Scientific, Waltham, MA, USA). Cells were maintained at 37 °C in a humidified incubator with 5% CO<sub>2</sub>.

### Real-time cell proliferation and drug IC<sub>50</sub> assessment using xCELLigence RTCA system

The xCELLigence real-time cell analysis (RTCA) system (Roche Applied Science, Indianapolis, IN, USA) was used to assess cell proliferation and determine drug IC<sub>50</sub> values through cell-impedance variation. The experiment began by adding 50 µl of DMEM supplemented with 10% FBS to each well of the E-plate 96 (ACEA Biosciences, San Diego, CA,

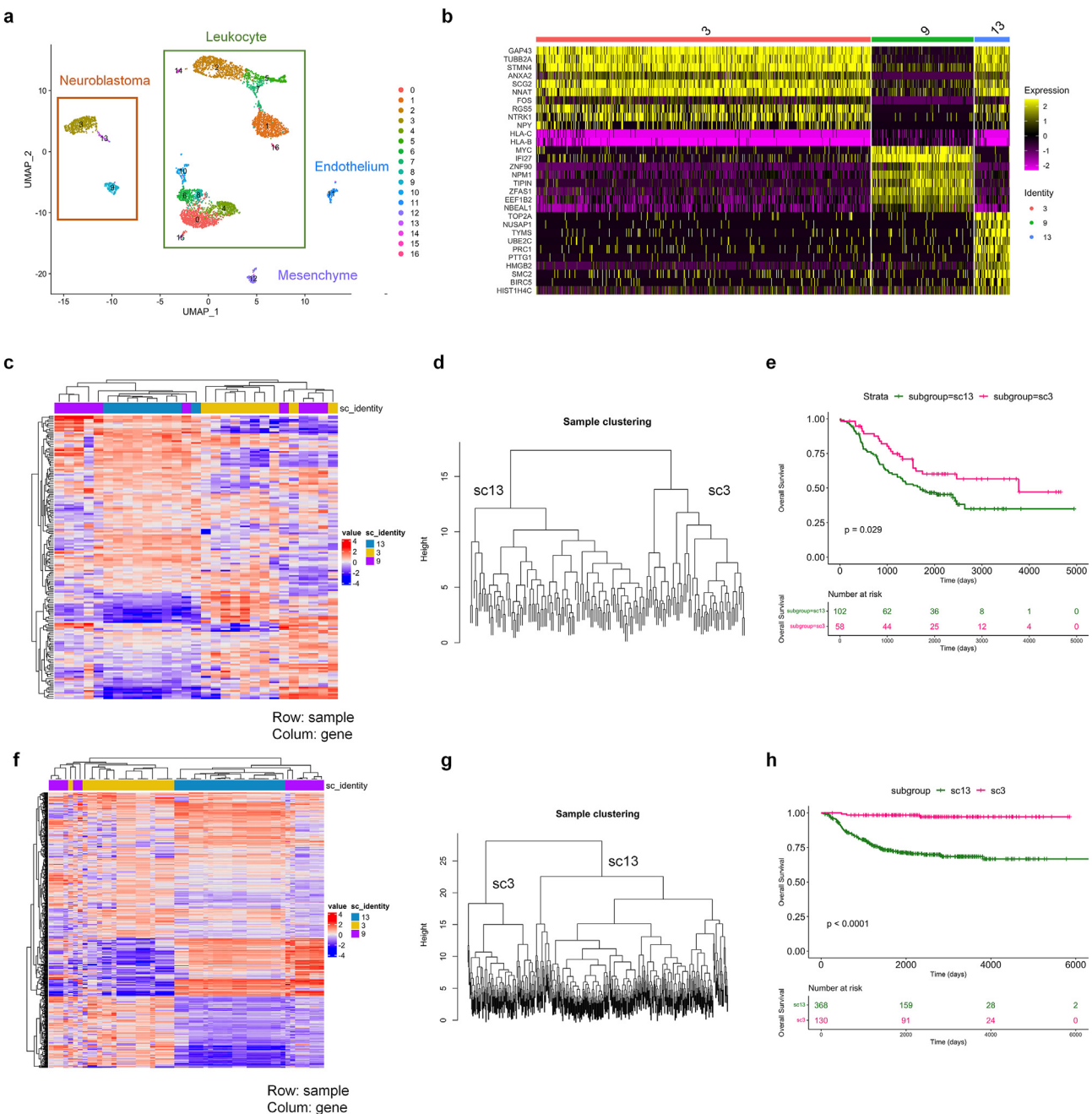


**Fig. 1.** Screening for drugs targeting high-risk neuroblastoma using single-cell RNA sequencing data. (a) 6442 cells from 5 neuroblastoma patients are projected on UMAP and can be divided into 4 major cell types including, neuroblastoma, leukocyte, mesenchyme and endothelium. (b) Heatmap presented the expression profile of top 10 differentially expressed genes (DEGs) from three neuroblastoma clusters which were further taken as cluster identity. (c) Heatmap revealed the expression level of 30 DEGs in 127 bulk neuroblastoma patient samples and the heterogeneity between patients from TARGET cohort. (d) The hierarchical clustering result of 127 bulk samples showed two distinct group of patients, which are named as cluster 13 and cluster 3, respectively. (e) Kaplan-Meier survival analysis revealed cluster 13 patients had significantly poorer overall survival rate than cluster 3 patients which illustrated that cell in cluster 13 were more malignant than cluster 3. (f) Heatmap revealed the expression level of 30 DEGs in 498 bulk neuroblastoma patient samples and the heterogeneity between patients from SEQC-NB498 dataset. (g) The hierarchical clustering result of 498 bulk samples showed two distinct group of patients, which are named as cluster 3 and cluster 13, respectively. (h) Kaplan-Meier survival analysis revealed cluster 13 patients had significantly poorer overall survival rate than cluster 3 patients which illustrated that cell in cluster 13 were more malignant than cluster 3.

USA), followed by connection to the system for baseline impedance readings. Subsequently, 50  $\mu$ l of medium and 50  $\mu$ l of cells (5000 cells per well) were added. After 24 h of cell seeding, Adavosertib, Vorinostat, Navitoclax, Entinostate, Leflunomide, ABT737 (HY-10993, HY-10221, HY-10087, HY-12163, HY-B0083; MedChemExpress, Monmouth Junction, NJ, USA), and Camptothecin (T1123; TargetMol, Wellesley Hills,

MA, USA) were serially diluted in triplicate (100  $\mu$ l per dilution) and added to the wells. The xCELLigence RTCA Software 2.0 (Roche Applied Sciences, Indianapolis, IN, USA) was utilized to monitor the normalized cell index and calculate the IC<sub>50</sub> values. Measurements were recorded hourly, and drug concentrations were sequentially diluted based on the IC<sub>50</sub> values of SK-N-DZ cells from the GDSC database.

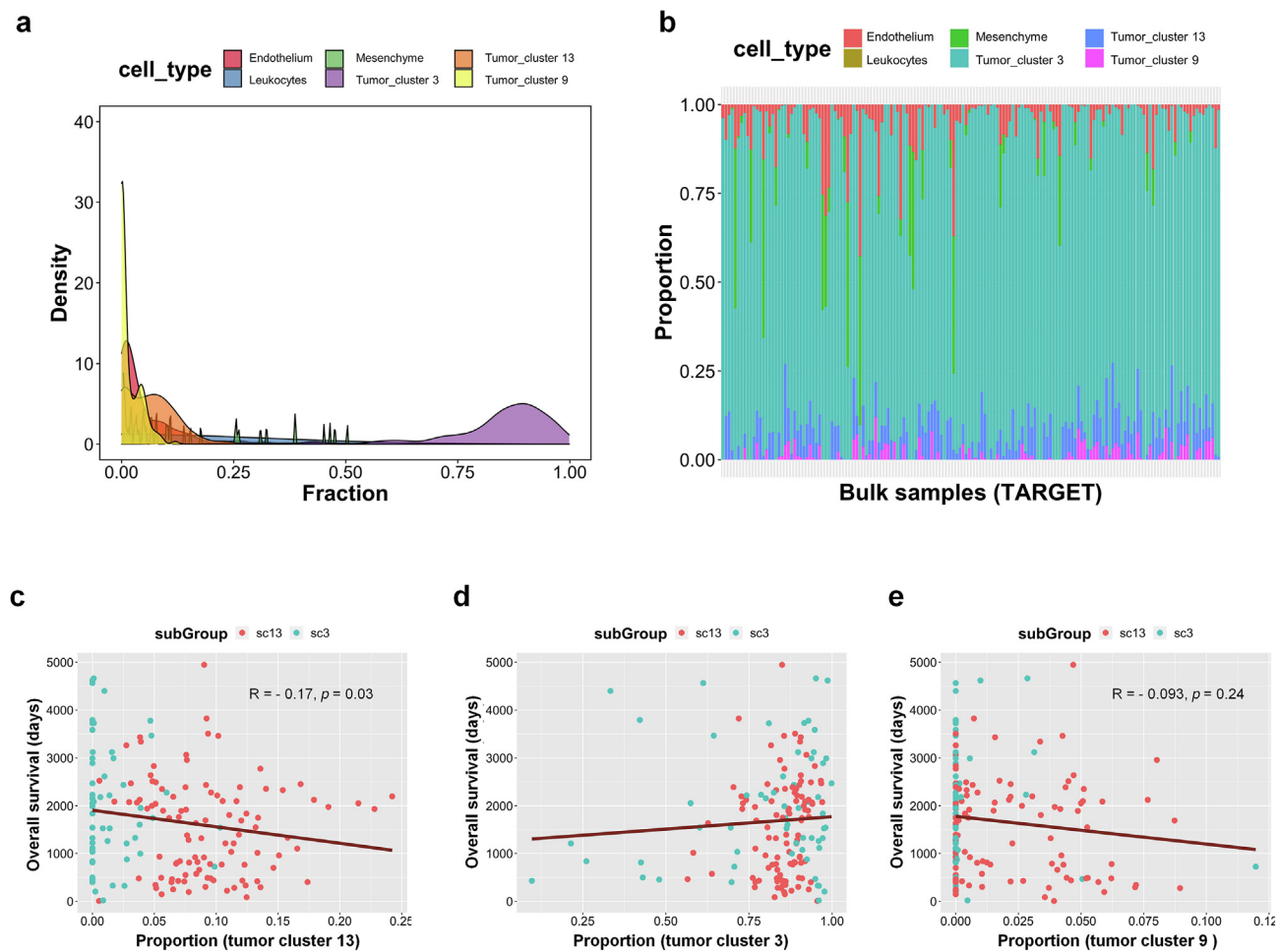


**Fig. 2.** Deciphering cellular dynamics and prognostic significance in tumor clusters. (a) Ridge plot revealed the density distribution of each cell type composition in 178 samples where tumor cluster 3 density were in the majority. (b) The bar plot showed the cell type composition of each sample. (c), (d), and (e) The relationship between overall survival and three tumor clusters, 3, 9 and 13, respectively where the cluster 13 proportion has significantly negative correlation with overall survival, in contrast, the cluster 3 has positive correlation with overall survival, showing that the cluster 13 was more malignant than cluster 3.

#### RNA extraction, cDNA synthesis, and quantitative real-time PCR (RT-qPCR) analysis

Samples were homogenized using TRIzol reagent (Thermo Scientific, Waltham, MA, USA), and total RNA was extracted using the Direct-zol<sup>TM</sup> RNA Miniprep kit (ZYMO research, Irvine, CA, USA). RNA concentration and quality were assessed with the NanoDrop ND-1000 (NanoDrop Technologies). For each sample, 100 ng of total RNA were reverse transcribed into cDNA using the RevertAid<sup>TM</sup> H Minus First Strand cDNA Synthesis Kit (Thermo Scientific, Waltham, MA, USA). mRNA levels were quantified through real-time PCR using cDNA-specific primers and iQ<sup>TM</sup>SYBR<sup>®</sup> Green Supermix #1708880 (Bio-Rad, Hercules, CA, USA). The mRNA expression was measured with Bio-Rad CFX Maestro (Bio-Rad, Hercules, CA, USA). Primer sequences used in the study are listed in Supplementary Table S1.

#### Plasmid transfection and overexpression validation in SK-N-DZ cells

SK-N-DZ cells were seeded at a density of  $4 \times 10^5$  cells per well in a six-well plate and incubated for 24 h. The cells were then transfected with 4  $\mu$ g of either control plasmid, UBE2C plasmid, or PTTG1 plasmid (Genescrypt, Piscataway, NJ, USA) using Lipofectamine 3000 (Thermo Fisher Scientific, Waltham, MA, USA) in 250  $\mu$ L of serum-free medium. After 6 h, the medium was replaced with serum-containing medium. After 24 h of transfection, G418 (Thermo Fisher Scientific, Waltham, MA,

USA) was added to select for cells that successfully incorporated the UBE2C plasmid or PTTG1 plasmid. Overexpression efficiency was confirmed through western blot analysis.

#### Cell cycle analysis following adavosertib treatment using flow cytometry

A total of  $1 \times 10^6$  SK-N-DZ cells were seeded in a 10 cm plate and incubated for 24 h, followed by treatment with Adavosertib for 24 h at IC<sub>50</sub> concentrations. The cells were then harvested, fixed in 70% ethanol overnight, and resuspended in PBS containing 100  $\mu$ g/mL RNase A and 0.1% Triton X-100. After staining with 5  $\mu$ g/mL propidium iodide for 1 h at 37 °C, the samples were analyzed using the FACSCanto flow cytometer (BD Biosciences, Franklin Lakes, NJ, USA).

#### Apoptosis analysis using annexin V-FITC/PI staining and flow cytometry

A total of  $2 \times 10^6$  SK-N-DZ cells were seeded in a 10 cm plate and incubated for 24 h, followed by treatment with Adavosertib for 48 h at IC<sub>50</sub> values concentrations. After treatment, the cells were washed, trypsinized, collected, and resuspend in PBS buffer. Next, 2  $\mu$ L of Annexin V-FITC reagent and 2  $\mu$ L of PI reagent (BD Biosciences, Franklin Lake, NJ, USA) were added to 100  $\mu$ L of the cell suspension and incubated for 15 min in the dark. Finally, 400  $\mu$ L of Annexin V binding buffer was added. The samples were then analyzed using the FACSCanto flow cytometer (BD Biosciences, Franklin Lake, NJ, USA).

### Western blot analysis

Cells were lysed using RIPA buffer (50 mM Tris-HCl, pH 7.4, 1% NP40, 0.1% SDS, 150 mM NaCl, and 0.5% sodium deoxycholate) supplemented with protease inhibitors. The lysates were centrifuged to remove debris, and the supernatants were collected after sonication for 2 min on ice using the Labsonic® M ultrasonic homogenizer (Sartorius AG). The samples were then centrifuged at 16,000×g for 15 min at 4 °C. Supernatants were collected, and protein concentrations were measured using a protein assay dye reagent (Bio-Rad, Hercules, CA, USA). Subsequently, 20 µg of protein from each sample was separated by SDS-PAGE and transferred onto a hydrophobic polyvinylidene difluoride (PVDF) membrane (Millipore, Burlington, MA, USA). Membranes were blocked with 1% bovine serum albumin in PBST and incubated overnight at 4 °C with primary antibodies against AKT, p-AKT, mTOR, p-mTOR, UBE2C, PTTG1, Cyclin B1, PARP, CDC2, p-CDC2, Caspase 3 (GTX110613, GTX128414, GTX1011557, GTX132803, GTX100599, GTX111938, GTX100911, GTX112864, GTX108120, GTX128155, GTX110543; GeneTex, Irvine, CA, USA) or β-actin (1:10,000 dilution; Millipore, Burlington, MA, USA). Afterward, membranes were incubated with

anti-rabbit/mouse IgG-HRP secondary antibodies (Abcam, Waltham, MA, USA) for 2 h at room temperature. Visualization was performed using ECL substrate (Advansta, Menlo Park, CA, USA) and images were captured with the FluorChem M system (ProteinSimple, San Jose, CA, USA).

### Cell migration assay using transwell chamber

A total of  $7 \times 10^5$  cells was suspended in serum-free DMEM and seeded into the upper chamber of a transwell (Corning, NY, USA). The lower chamber was filled with 600 µL DMEM supplemented with 10% FBS. After a 12 h incubating, the cells were fixed with methanol and stained with crystal violet (Sigma-Aldrich, St. Louis, MO, USA). Cell migration was qualified by counting the stained cells in five randomly selected fields.

### Statistical analysis

All data are presented as mean ± standard deviation (SD) unless stated otherwise. A student's *t*-test was conducted to evaluate the

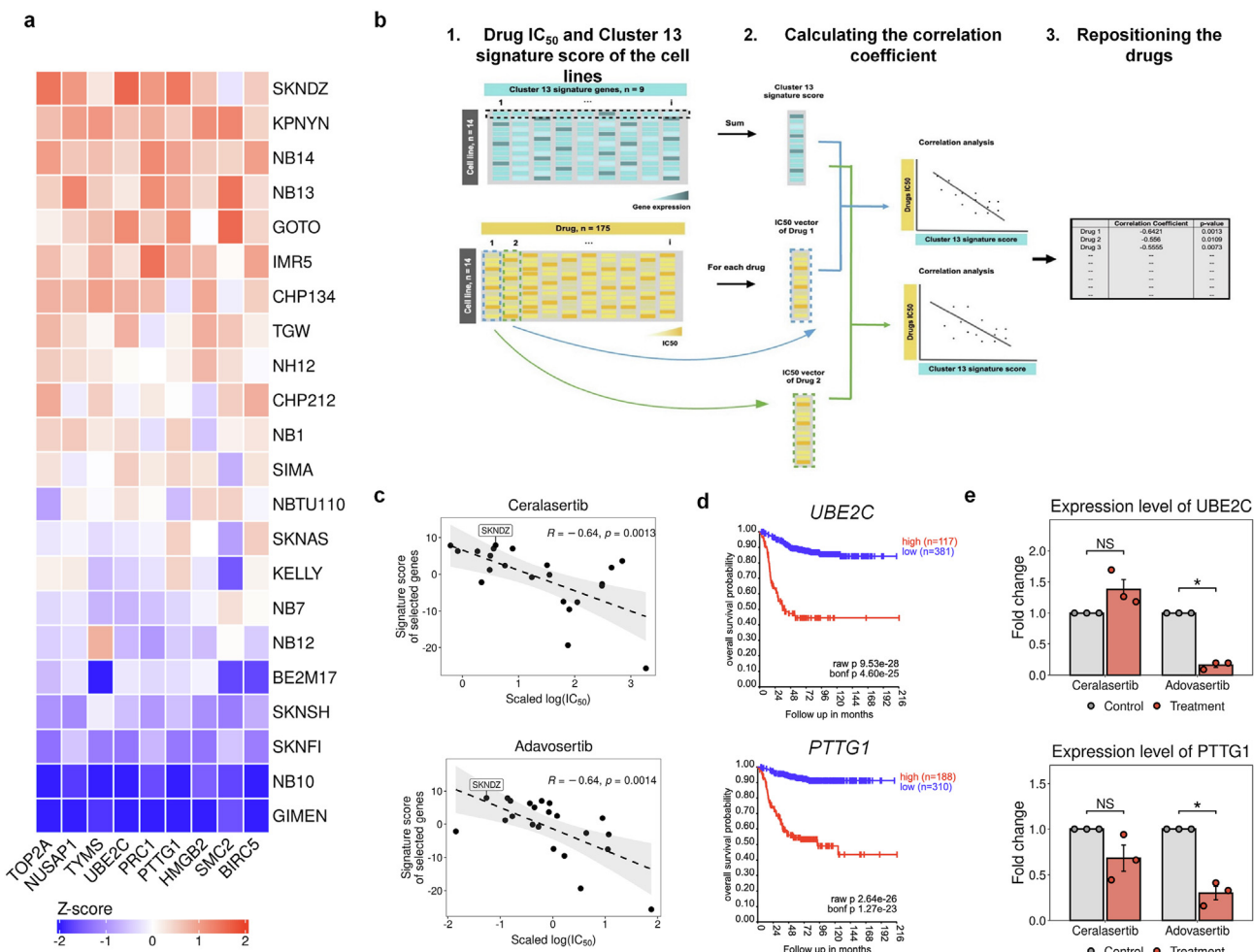


**Fig. 3.** Identification of signature genes and drug candidates targeting cluster 13 in neuroblastoma cell lines. (a) The heatmap revealed the expression level of nine signature genes in each neuroblastoma cell line where SK-N-DZ was selected for further analysis and experiment. (b) (1) In 14 cell lines, the scaled expression values of 9 Differentially Expressed Genes (DEGs) are summed up to obtain the respective cluster 13 scores. The Drug IC<sub>50</sub> values for different cell lines are sourced from the GDSC datasets. (2) To identify drugs that target cluster 13, a correlation coefficient is calculated between the IC<sub>50</sub> vectors of 175 drugs across the 14 cell lines and the cluster 13 scores. (3) The drugs with significant negative correlations are considered as potential candidates that target cluster 13. These drugs are then filtered out for further investigation as they may exhibit specific effects on the biological processes related to cluster 13 in the given cell lines. (c) The scatter plot of top two drug candidates, Ceralasertib and Adavosertib, showed significantly negative correlation between signature score and scaled log(IC<sub>50</sub>) in cell lines. (d) Kaplan-Meier survival analysis identified top two genes, UBE2C and PTTG1, where the survival time of patients with high expression of UBE2C and PTTG1 is lower than the patients with low expression, and we treated UBE2C and PTTG1 as drug targets. (e) Adavosertib significantly reduced UBE2C and PTTG1 levels compared to Ceralasertib, making Adavosertib the chose drug candidate for further experiments.

difference between two groups, with statistical significance defined as  $P < 0.05$ . All experiments were performed with at least three biological replicates and three technical replicates.

## Results

### *Identification and characterization of distinct malignant neuroblastoma clusters using single-cell transcriptomics reveals malignant subpopulations associated with poor survival*

We conduct single-cell transcriptomic analysis, combining clustering of bulk neuroblastoma cohorts and deconvolution of bulk RNA-seq data to identify and characterize malignant neuroblastoma clusters. The pre-processed single-cell transcriptomes from the Neuroblastoma Cell Atlas were downloaded, and a total of 6442 cells derived from 5 patients were analyzed. We applied quality control to filter out low-quality cells. Feature selection was then employed to identify genes with highly differential expression, and highly variable genes were selected for principal component analysis (Supplemental Fig. S1). Subsequently, data were subjected to UMAP, a nonlinear dimension reduction method. Based on well-known neuroblastoma related marker genes, including leukocyte (*PTPRC*), mesenchymal (*TCF21*, *PDGFRB*), endothelium (*KDR*, *PECAM1*, *PLVAP* and *PTPRB*) and neuroblastoma (*PHOX2A*, *PHOX2B* and *MYCN*), cells were annotated with four distinct cell types (Fig. 1a). Pairwise comparisons were performed between the tumor clusters, resulting in top 10 differentially expressed genes (DEGs) of each cluster that represented the characteristics of each tumor cluster (Fig. 1b).

To connect the single cell clustering result with clinical information, we collected 127 patient samples from TARGET cohort and conducted hierarchical clustering based on the top 10 DEGs from cluster 3, 9 and 13, respectively. The results revealed the presence of two distinct clusters of neuroblastoma patients, which are further named as cluster 3 and cluster 13. Therefore, we concluded that neuroblastoma patients can be classified into two distinct clusters using single-cell data, and linked with clinical information to unveil the malignancy of each single-cell cluster (Fig. 1c and d).

In the context of tumor heterogeneity, Kaplan-Meier curves were plotted using the TARGET data to investigate the survival rates of cluster 13 and cluster 3. The result clearly shows that cluster 13 is more malignant than cluster 3 (Fig. 1e). To further confirm the association between the signature genes of each cluster and hierarchical clustering was conducted using samples from SEQC (Fig. 1f and g). The group with high expression of signature 13 genes exhibited lower overall survival rate compared to the group with low expression of signature 13 genes (Fig. 1h).

### *Deconvolution of neuroblastoma cell types reveals cluster 13 as a malignant subpopulation correlated with poor overall survival*

We further applied CIBERSORTx to perform deconvolution analysis, utilizing single-cell transcriptomic data as the reference to estimate the cell type composition in each patient sample. This analysis identified six distinct cell groups, which included three different neuroblastoma

**Table 2**  
Correlation coefficient of cluster 13 score and IC<sub>50</sub>.

drug	coeff_13	p_13
Ceralasertib	-0.6421	0.001274
Adavosertib	-0.63815	0.001395
Leflunomide	-0.6029	0.008086
Vorinostat	-0.60044	0.00313
Sorafenib	-0.59009	0.003842
Etinostat	-0.57682	0.012207
Navitoclax	-0.55604	0.010903
VE-822	-0.55555	0.016683
ABT737	-0.55499	0.007341
Camptothecin	-0.55276	0.007631
Ruxolitinib	-0.5384	0.021162
Obatoclax Mesylate	-0.53538	0.022038
PCI-34051	-0.51479	0.028814
MN-64	-0.51164	0.029975
PFI3	-0.4999	0.034641
Vinorelbine	-0.49312	0.027154
Irinotecan	-0.48716	0.021474
XAV939	-0.48519	0.041254
Alisertib	-0.47877	0.044422
Cisplatin	-0.47285	0.026253
WEHI-539	-0.46671	0.028548
Pevonedistat	-0.46275	0.03011
LY2109761	-0.45818	0.055849
VE821	-0.45078	0.046072

clusters. The density distribution of these clusters across all patient samples was visualized using a ridge plot, showing that tumor cluster 3 was the predominant cell population. A bar plot was also generated to display the detailed cell type composition for each sample (Fig. 2a and b).

To assess the malignancy of each neuroblastoma cluster, we examined the correlation between the proportion of cells in each cluster and overall patient survival time. A statistically significant negative correlation was observed between the proportion of cluster 13 cells and overall survival (Fig. 2c), indicating that a higher abundance of cluster 13 cells is associated with a poorer prognosis. In contrast, clusters 3 and 9 showed no significant relationship with survival outcomes (Fig. 2d and e), further emphasizing the aggressive nature of cluster 13 compared to the other two clusters. These findings highlight the critical role of cluster 13 in neuroblastoma progression and its potential as a therapeutic target.

### *Identification of adavosertib as a promising therapeutic candidate targeting malignant neuroblastoma cluster 13 through gene signature analysis and drug screening*

To identify potential therapeutic candidates targeting malignant neuroblastoma cells, we first began by selecting a representative cell line that closely mimicked the malignant characteristics of cluster 13. The expression levels of nine signature genes were assessed across various neuroblastoma cell lines (Fig. 3a). Using the signature score of cluster 13, calculated as the sum of scaled expression values for these 9 genes, we identified SK-N-DZ as the cell line the highest similarity to cluster 13, making it suitable for further analysis and experiment (Table 1).

**Table 1**  
Cluster 13 signature score.

TOP2A	NUSAP1	TYMS	UBE2C	PRC1	PTTG1	HMGB2	SMC2	BIRC5	cell_line	total
1.478865	1.084612	0.292596	1.605172	1.085588	1.42841	0.661082	-0.25	0.545438	SKNDZ	7.931765
0.696743	1.0163	1.103796	0.659408	0.886524	0.566356	1.176623	1.272288	0.473533	KPNYN	7.85157
1.025026	0.609116	0.684296	0.456587	1.23096	0.980135	0.555434	0.472854	1.005908	NB14	7.020314
0.516957	1.276564	0.555848	0.253211	1.199719	0.89219	0.458394	1.467138	0.39946	NB13	7.019481
0.17591	0.480913	0.715557	1.225279	0.555599	1.154336	-0.02283	1.588224	0.468777	GOTO	6.341764
0.679059	0.27999	0.861073	0.335541	1.507985	0.863964	0.732684	0.069065	0.959219	IMR5	6.288581
0.805523	0.721532	0.99663	0.816336	0.732839	-0.26813	0.920775	-0.15156	0.518933	CHP134	5.092881
0.76911	0.375899	0.109656	0.826841	-0.24574	0.160807	0.858535	0.620726	0.194652	TGW	3.670482
0.556604	0.37721	0.271547	0.049202	-0.00108	0.187997	0.745031	0.354955	-0.04473	NH12	2.496731
0.310458	-0.18277	-0.02584	0.534458	0.235511	0.452142	0.304301	-0.75071	0.30588	SIMA	1.183429
0.162571	0.224668	-0.62875	-0.45178	-0.27082	0.47724	-0.2352	-1.59174	0.134466	KELLY	-2.17934

Next, we developed a framework to identify personalized therapeutic candidates for malignant neuroblastoma. We conducted a correlation analysis between the drug response score of 175 compounds and the cluster 13 signature score to pinpoint drugs with potential efficacy against malignant tumors (Fig. 3b). Among the 14 neuroblastoma cell lines in GDSC database, we calculated the signature score of cluster 13 and revealed the top 10 drugs with a significant correlation (Table 2). The top 2 candidates, Ceralasertib and Adavosertib, both showed correlation coefficients below  $-0.6$ , indicating strong potential as therapeutic agents for the malignant cluster (Fig. 3c).

Furthermore, we performed survival analysis using the SEQC-NB498 database for each of the nine signature gene in cluster 13. All of these genes were significantly associated with poorer patient outcomes (Supplemental Fig. S2a), suggesting that patients with higher expression levels of these genes had a worse prognosis (Supplemental Fig. S2b). We then focused on UBE2C and PTTG1, the two most significant genes based on the p value ranking in the survival analysis (Fig. 3d). Finally, we conducted qPCR experiment and observed that only Adavosertib significantly down-regulated the expression of UBE2C and PTTG1 (Fig. 3e). Thus, we identified Adavosertib as a promising novel therapeutic candidate for targeting malignant neuroblastoma cells.

#### Adavosertib effectively inhibits cell proliferation and induces apoptosis in malignant neuroblastoma cells by targeting the AKT/mTOR pathway and causing G2/M phase arrest

After identifying Adavosertib as a potential therapeutic candidate, we evaluated its efficacy using the RTCA system. The results showed that Adavosertib effectively inhibited the proliferation of SK-N-DZ cells. Additionally, as the concentration of the drug increased, a notable reduction in cell viability was observed. Adavosertib, also known as AZD1775 and MK-1775, exhibited an  $IC_{50}$  value of  $0.045\ \mu M$  in SK-N-DZ cells, indicating high potency and a strong inhibitory effect (Fig. 4a and Table 2). Previous studies have shown that Adavosertib can bypass S and G2/M phase checkpoints, leading to premature mitotic entry, mitotic catastrophe, and subsequent cell death in various cancer models [23].

To explore the regulatory impact of Adavosertib on the AKT/mTOR signaling pathway, we analyzed the expressions of p-AKT/AKT and p-mTOR/mTOR proteins. Adavosertib treatment resulted in a dose-dependent reduction of these protein expression levels, demonstrating that the drug exerts its inhibitory effect on cell proliferation by suppressing the AKT/mTOR pathway (Fig. 4b and c). This pathway is crucial for regulating cell cycle progression, and the transition through the G2/M phase is tightly controlled by the CDC2/Cyclin B1 complex. Flow cytometric analysis further revealed a significant increase in the percentage

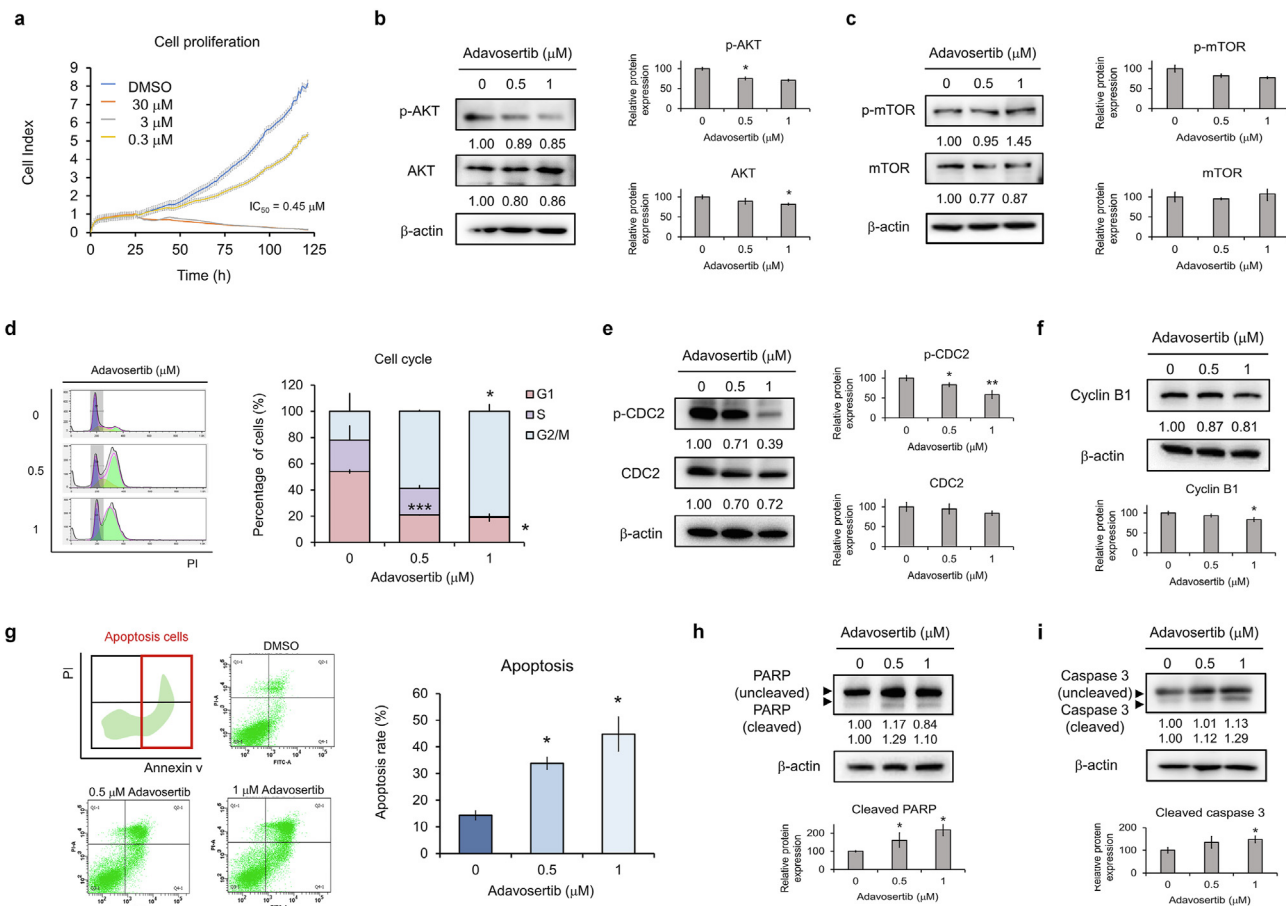


**Fig. 4.** Effect of Adavosertib in SK-N-DZ neuroblastoma cell line. Among the ten drugs selected from the single-cell data, Adavosertib is known to modulate the AKT/mTOR pathway, thereby influencing cell proliferation, cell cycle progression, and apoptosis. (a) RTCA was also utilized to measure Adavosertib effects in SK-N-DZ cells. (b) and (c) Western blot analysis of p-AKT, AKT, p-mTOR, and mTOR protein expression after 24 h Adavosertib treatment in SK-N-DZ cells. (d) Cell cycle analysis in SK-N-DZ cells treated with  $0.5\ \mu M$  and  $1.0\ \mu M$  Adavosertib for 24 h, revealing a significant increase in the G2/M phase. (e) and (f) Western blot analysis of p-CDC2, CDC2, and Cyclin B1 protein expression post-Adavosertib treatment. (g) Cell apoptosis analysis in SK-N-DZ cells after 48 h Adavosertib treatment, showing a significant increase in apoptotic cell populations. (h) and (i) Western blot analysis depicting elevated expression levels of apoptosis-associated proteins (Caspase 3 and PARP) in SK-N-DZ cells treated with Adavosertib for 24 h at concentrations of  $0.5\ \mu M$  and  $1.0\ \mu M$ . Experiments were conducted in triplicate, and a representative experiment is presented.  $\beta$ -actin expression served as the loading control. Data are expressed as mean  $\pm$  SD from three independent, triplicate experiments. \* $P < 0.05$ , \*\* $P < 0.001$ .

of cells in the G2/M phase after a 24 h with Adavosertib treatment (Fig. 4d). This observation was supported by the downregulation of p-CDC2, CDC2, and Cyclin B1 expression levels, suggesting that Adavosertib induces G2/M arrest through inhibition of the CDC2/Cyclin B1 complex (Fig. 4e and f).

When cells experience severe damage, they may undergo cell cycle arrest and eventually apoptosis. Flow cytometric analysis demonstrated a substantial increase in apoptotic cells following 48 h of davoosertib treatment (Fig. 4g). To further confirm the induction of apoptosis by Adavosertib, we examined the protein levels of Poly (ADP-ribose) Polymerase (PARP) and caspase 3, two key markers of apoptosis, using Western blot analysis. Both PARP and caspase 3 levels were significantly elevated after a 24 h with Adavosertib treatment, indicating enhanced apoptosis induction (Fig. 4h and i). These findings support the potential of Adavosertib as an effective therapeutic agent in targeting malignant neuroblastoma cells.

#### *Overexpression of UBE2C and PTTG1 activates the AKT/mTOR pathway and reduces the anti-proliferative effect of adavosertib in malignant neuroblastoma cells*

Following the observation that Adavosertib promotes apoptosis and induces G2/M arrest, we further investigate its effect on the expression levels of cluster 13 signature genes. RT-qPCR analysis revealed that the

mRNA levels of five out of nine cluster 13 signature genes were significantly reduced in SK-N-DZ cells after Adavosertib treatment. Among these genes, UBE2C and PTTG1 exhibited the highest cluster 13 signature scores making them the focus of our subsequent investigation to understand their roles in modulating the response to Adavosertib.

We first confirmed the successful overexpression of UBE2C and PTTG1 in SK-N-DZ cells through western blot analysis (Fig. 5a and b). Since excessive activation of the AKT/mTOR pathway has been linked to drug resistance and tumor progression. To exam the influence of UBE2C and PTTG1 overexpression on the AKT/mTOR pathway, we examined the impact of UBE2C and PTTG1 overexpression on this pathway. Results showed that overexpression of UBE2C and PTTG1 led to increased levels of p-AKT, AKT, p-mTOR, and mTOR proteins, regardless of Adavosertib treatment (Fig. 5c-f). This upregulation of AKT/mTOR pathway promoted cell proliferation and counteracted the inhibitory effect of Adavosertib on cell growth, suggesting that UBE2C and PTTG1 play a crucial role in diminishing the drug's efficacy in malignant neuroblastoma cells.

#### *UBE2C and PTTG1 differentially modulate adavosertib-induced G2/M arrest and apoptosis while enhancing migration and invasion in malignant neuroblastoma cells*

Next, we investigated how the overexpression of UBE2C and PTTG1 influences the G2/M arrest induced by Adavosertib. Flow cytometric

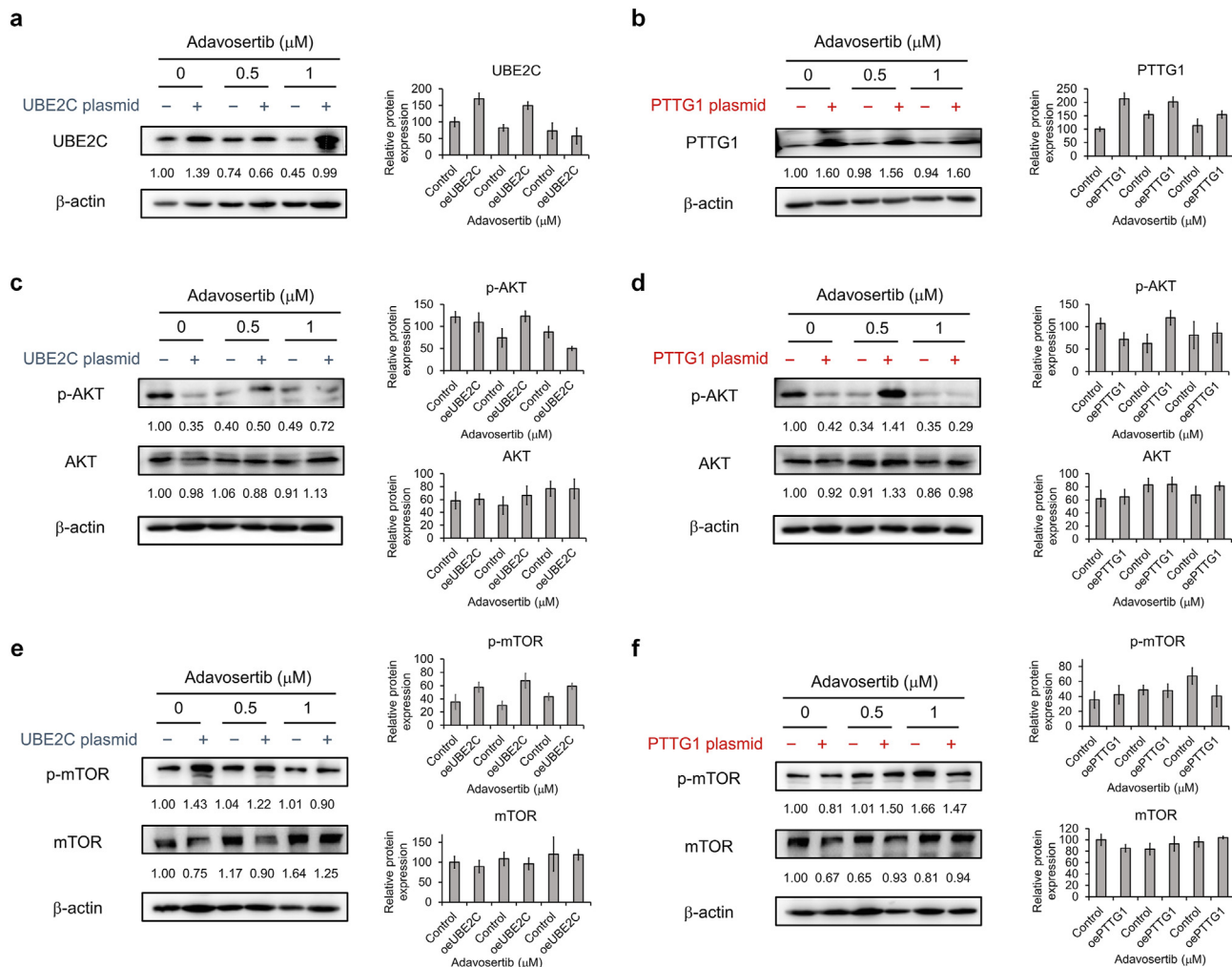


**Fig. 5.** Overexpression of UBE2C and PTTG1 resulted in the hyperactivation of the AKT/mTOR pathway. (a) qRT-qPCR analysis was performed to evaluate the mRNA levels in SK-N-DZ cells following a 24 h treatment with IC<sub>50</sub> doses of Adavosertib. (b–g) Western blot analysis of UBE2C, PTTG1, p-AKT, AKT, p-mTOR and mTOR protein levels in SK-N-DZ cells. The experiments were performed in triplicate, and a representative experiment is presented. The expression of β-actin was used as the loading control. The results were expressed as the mean ± SD of three independent experiments. The results are represented as the mean ± SD of three independent experiments. Statistical significance is denoted as \*P < 0.05 and \*\*P < 0.01.

analysis showed that without drug treatment, overexpression of either UBE2C or PTTG1 alleviated the G2/M arrest caused by Adavosertib. However, after 24 h of treatment with 0.5  $\mu$ M Adavosertib, only UBE2C-overexpressing cells exhibited a significant reduction in the proportion of cells arrested at the G2/M phase (Fig. 6a). This finding led us to hypothesize that UBE2C and PTTG1 might have distinct effects on the CDC2/cyclin B1 complex. Western blot analysis confirmed that the expression levels of CDC2 and Cyclin B1 were elevated in UBE2C-overexpressing cells, regardless of drug treatment, compared to the control cells (Fig. 6b–e). This pattern was not observed in PTTG1-overexpressing cells, suggesting that UBE2C can counteract the G2/M arrest induced by Adavosertib through upregulation of CDC2 and Cyclin B1, whereas PTTG1 lacks this capability. Notably, in PTTG1-overexpressing cells treated with 0.5  $\mu$ M and 1.0  $\mu$ M Adavosertib, CDC2 levels decreased, and the incidence of G2/M arrest increased compared to the control group.

To further understand the effects of UBE2C and PTTG1 overexpression on apoptosis, we treated cells with Adavosertib for 48 h and performed flow cytometry analysis. Regardless of drug treatment, cells overexpressing UBE2C showed significantly lower levels of apoptosis compared to the control group (Fig. 7a). In contrast, PTTG1-overexpressing cells only exhibited lower apoptosis rates in the absence of Adavosertib. Additionally, both UBE2C and PTTG1 overexpression resulted in a marked decrease in apoptosis-associated proteins, such as caspase 3 and PARP (Fig. 7b–e). These results suggest that

UBE2C and PTTG1 can attenuate the apoptotic effects induced by Adavosertib.

Since cell migration is a key factor in cancer progression, we also evaluated the impact of Adavosertib in SK-N-DZ neuroblastoma cell migration using transwell assays at the IC<sub>50</sub> concentrations. Adavosertib treatment significantly reduced migration activity of SK-N-DZ (Fig. 8a). However, overexpression of UBE2C and PTTG1 significantly enhanced the migratory capacity of SK-N-DZ cells, both with and without Adavosertib treatment (Fig. 8b). Collectively, the results from the cell-based experiments demonstrate that Adavosertib inhibits cell proliferation, induces G2/M phase arrest, promotes apoptosis, and reduces migration and invasion ability in malignant neuroblastoma.

## Discussion

This study was driven by the clinical challenge posed by the extensive heterogeneity observed in neuroblastoma. To tackle this issue, we utilized single-cell transcriptomic data to identify potential therapeutic agents that can specifically targeting malignant tumor subpopulations and elucidate their mechanisms of action. Our analysis, which involved preprocessing single-cell transcriptomes from the Neuroblastoma Cell Atlas, resulting in 6442 cells derived from 5 patients. UMAP clustering revealed distinct tumor clusters, with cluster 13 showing significantly higher malignancy compared to cluster 3, as evidenced by Kaplan-Meier survival analysis. To further explore therapeutic options, SK-N-DZ cells

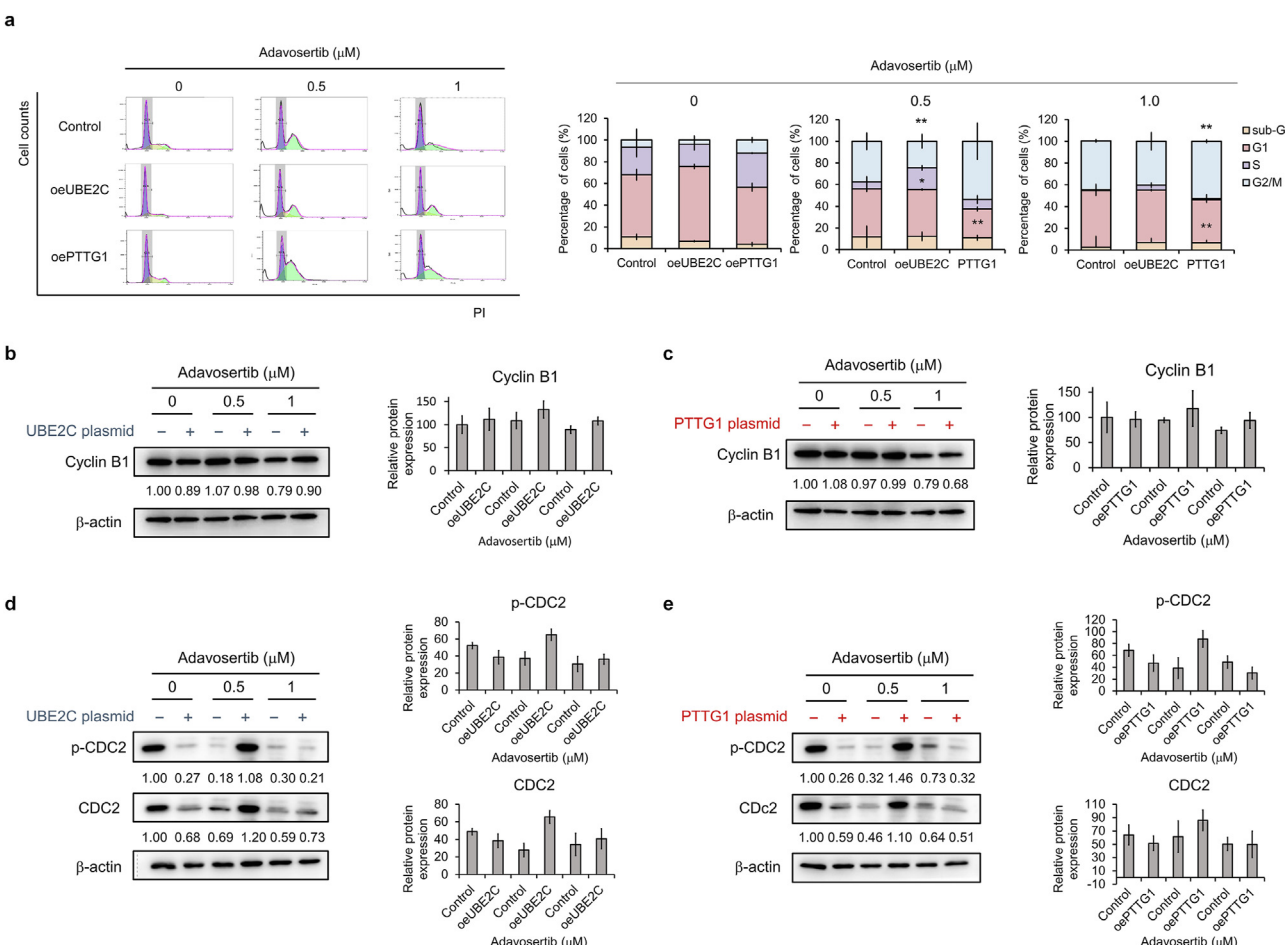


**Fig. 6.** Overexpression of UBE2C reduced Adavosertib-induced G2/M arrest. (a) Statistical analysis of cell percentage in G0/G1, S, G2/M Phases in SK-N-DZ cells with Control-Plasmid, UBE2C-Plasmid, or PTTG1-Plasmid infection after the treatments with Adavosertib for 24 h. (b–e) Western blot analysis of p-CDC2, CDC2 and Cyclin B1protein expression in SK-N-DZ cells with PTTG1 and UBE2C overexpressed cells after Adavosertib treatment for 24 h. The experiments were performed in triplicate, and a representative experiment is presented. Employing  $\beta$ -actin expression effectively functioned as the loading control. Data are shown as mean  $\pm$  standard error of mean (SEM). \* $P$  < 0.05, \*\* $P$  < 0.01.

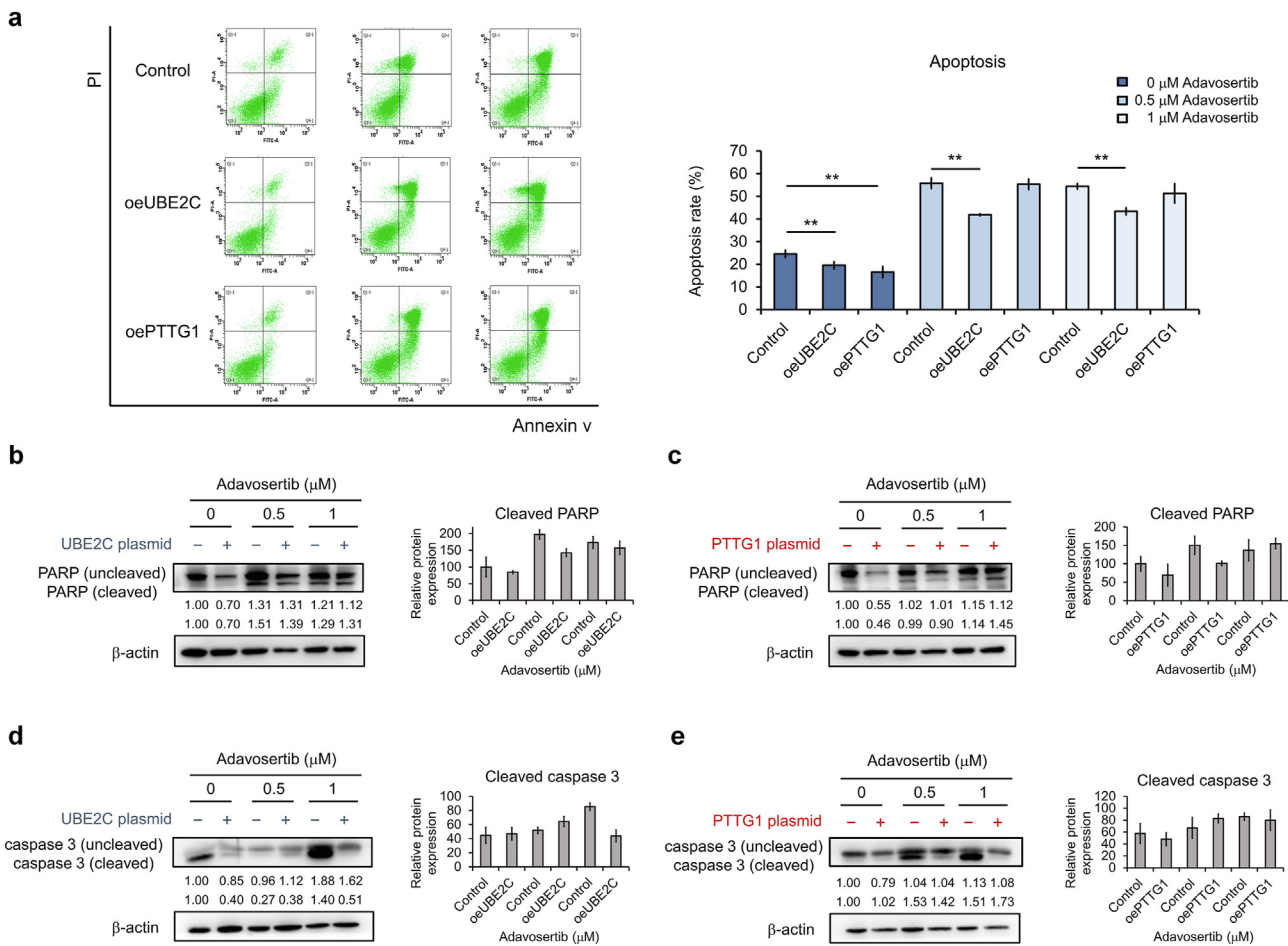


**Fig. 7.** Overexpression of UBE2C and PTTG1 reduced Adavosertib-induced apoptosis in absence of Adavosertib treatment. (a) Cell apoptosis analysis in SK-N-DZ with control-plasmid, UBE2C-plasmid, and PTTG1-plasmid treated with Adavosertib for 24 h. Data are shown as mean  $\pm$  SD from three independent, triplicate experiments. (b-e) Western blot analysis of Caspase 3 and PARP protein expression in SK-N-DZ cells with control-plasmid, UBE2C-plasmid, and PTTG1-plasmid after Adavosertib treatment for 24 h. The experiments were performed in triplicate, and a representative experiment is presented. The utilization of  $\beta$ -actin expression served its purpose as the loading control, and the results were represented as the mean  $\pm$  SD of three independent experiments. \*\* $P$  < 0.01.

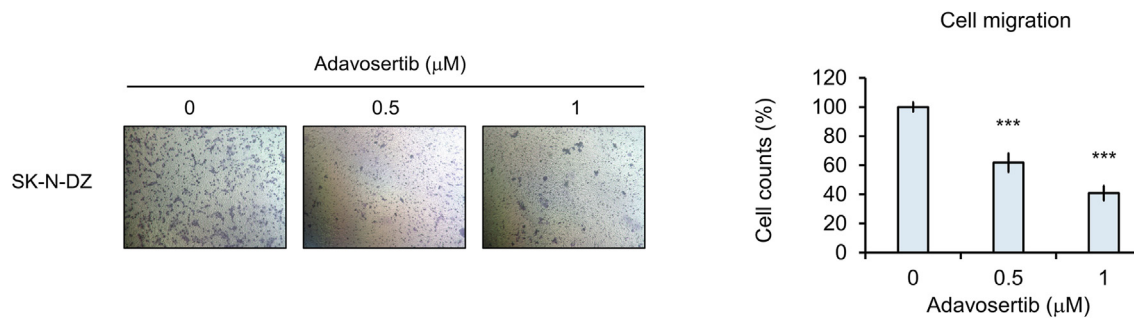
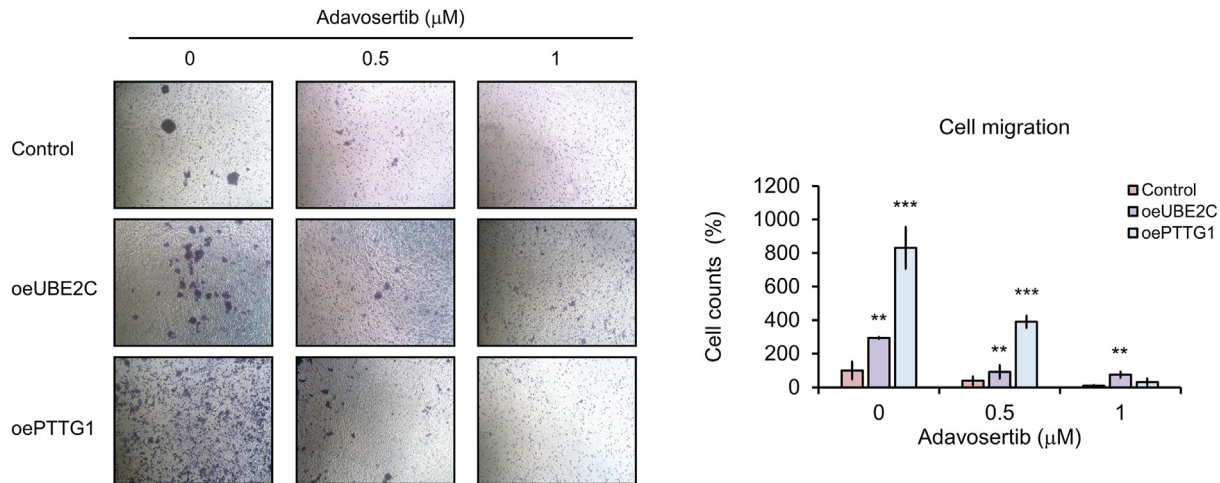
were selected to represent cluster 13 in subsequent drug screening, where we identified Adavosertib as the most effective candidate. Adavosertib, a WEE1 kinase inhibitor currently in Phase II clinical trials for pediatric solid tumors, including neuroblastoma [24–27], was shown to significantly inhibit cell proliferation by targeting the AKT/mTOR pathway, a key signaling cascade involved in neuroblastoma progression. Further studies will focus on exploring the impact of Adavosertib on cell cycle regulation and its ability to induce apoptosis in malignant neuroblastoma cells. Previous studies have shown that dysregulation of the AKT/mTOR pathway plays a critical role in the development and progression of neuroblastoma [28]. Consequently, our research aims to investigate whether Adavosertib influences tumor-related characteristics, such as cell cycle dysregulation, inhibition of p53-mediated apoptosis, and enhanced cell migration [29,30].

The CDC2/cyclin B complex is essential for G2/M phase checkpoint regulation [31]. Consistent with our findings, G2/M cell cycle arrest is often accompanied by a decrease in CDC2 and Cyclin B1 levels (Fig. 4). Adavosertib treatment led to a marked reduction in Cyclin B1 expression in SK-N-DZ cells, which indicates that the drug induces G2/M arrest by downregulating Cyclin B1 levels. These observations are consistent with previous research results, further supporting the potential of Adavosertib to disrupt cell cycle progression in neuroblastoma cells [32].

The examination of Adavosertib's impact on the differentially expressed genes (DEGs) within cluster 13 unveiled a significant decrease in the expression levels of UBE2C and PTTG1. UBE2C, a member of the

ubiquitin-conjugating enzyme (E2) family, plays a crucial role in protein degradation by delivering activated ubiquitin molecules to specific lysine residues on substrates, either directly or through an E3 ligase [33]. This enzyme plays a pivotal role in regulating cell cycle progression by tagging target proteins for proteasomal degradation. Overexpression of UBE2C has been shown to disrupt spindle checkpoint activity after mitotic entry, making it as a potential therapeutic target for cancer therapy. Conversely, downregulation of UBE2C has been associated with increased apoptosis and cell cycle arrest in various cancer cells, highlighting its significance in cancer research. Pituitary tumor transforming gene 1 (PTTG1), on the other hand, encodes a protein that functions as a separin inhibitor, suppressing the activity of separase, a protease critical for sister chromatid separation during mitosis [34,35]. Elevated PTTG1 levels have been observed in multiple cancer types, including breast, lung, prostate, and colon cancer, and are correlated with tumor development and progression. Inhibition of PTTG1 has been demonstrated to induce apoptosis and trigger cell cycle arrest, positioning it as an attractive therapeutic target for cancer therapy [36,37]. Together, these findings suggest that both UBE2C and PTTG1 are critical mediators of tumorigenesis and hold potential as therapeutic targets for neuroblastoma.

Our findings indicate that the overexpression of UBE2C and PTTG1 leads to hyperactivation of the AKT/mTOR pathway, a mechanism that has been implicated in drug resistance and cancer progression. This is consistent with previous studies showing that genetic alterations resulting in high levels of PTTG1 expression are significantly associated with

**a****b**

**Fig. 8.** Overexpression of UBE2C and PTTG1 enhanced cell migration. (a) The migration ability of SK-N-DZ cells after Adavosertib treatment was assessed using transwell assays. (b) The migration ability after overexpression of UBE2C and PTTG1 in SK-N-DZ cells after Adavosertib treatment was assessed using transwell assays. Data are shown as mean  $\pm$  SD from three independent, triplicate experiments. \*\* $P < 0.01$ , \*\*\* $P < 0.001$ .

poorer survival outcomes, which aligns with our observations in SK-N-DZ cells. Moreover, previous research has demonstrated that silencing UBE2C in human melanoma cells induces G2 phase arrest, and similar effects have been observed in pancreatic cancer cells, where UBE2C knockdown led to increased apoptosis [38,39]. Additionally, several studies have reported that both UBE2C and PTTG1 contribute to enhanced cell migration [40–42]. Our study further supports this by showing that the overexpression of UBE2C and PTTG1 in SK-N-DZ cells significantly increased their cell migration, an attribute commonly associated with aggressive cancer phenotypes. This evidence underscores the critical roles of UBE2C and PTTG1 in promoting malignancy and highlights their potential as therapeutic targets in neuroblastoma.

#### Author contributions

H-CH and H-FJ conceived the study. Y-XC and H-FJ designed the experiments. C-HH and Y-XC performed the experiments and data analyses. T-YT and AL performed the bioinformatics analysis. C-HH, Y-XC, H-CH, and H-FJ wrote the manuscript.

#### Data availability

The data supporting the findings of this study are available in the Methods and supplementary information section.

#### Funding

This work was supported by the National Science and Technology Council, Taiwan (112-2221-E-A49-061-MY3, 113-2320-B-002-025-MY3,

113-2221-E-002-149-MY3), the Higher Education Sprout Project (NTU-CC-113L894502, NTU-CC-113L890302, NTU-113L8503) and Center for Advanced Computing and Imaging in Biomedicine (NTU-112L900701, NTU-113L900701) from The Featured Areas Research Center Program within the framework of the Higher Education Sprout Project by the Ministry of Education (MOE), Taiwan.

#### Declaration of competing interest

The authors declare that they have no conflict of interest.

#### Acknowledgments

We acknowledge Technology Commons at the College of Life Science and Instrumentation center, National Taiwan University for technical assistance.

#### Appendix A. Supplementary data

Supplementary data to this article can be found online at <https://doi.org/10.1016/j.neurot.2025.e00575>.

#### References

- [1] Kamihara J, Bourdeaut F, Foulkes WD, Molenaar JJ, Mosse YP, Nakagawara A, et al. Retinoblastoma and neuroblastoma predisposition and surveillance. *Clin Cancer Res* 2017;23:e98–106.
- [2] Lucena JN, Alves MTS, Abib SCV, Souza GO, Neves RPC, Caran EMM. Clinical and epidemiological characteristics and survival outcomes of children with

- neuroblastoma: 21 years of experience at the instituto de oncología pediátrica, in são paulo, brazil. *Rev paul pediatr* 2018;36:254–60.
- [3] Matthay KK, Maris JM, Schleiermacher G, Nakagawara A, Mackall CL, Diller L, et al. Neuroblastoma. *Nat Rev Dis Primers* 2016;2:16078.
- [4] Cohn SL, Pearson AD, London WB, Monclair T, Ambros PF, Brodeur GM, et al. The international neuroblastoma risk group (INRG) classification system: an INRG task force report. *J Clin Oncol* 2009;27:289–97.
- [5] Moreno L, Caron H, Geerger B, Eggert A, Schleiermacher G, Brock P, et al. Accelerating drug development for neuroblastoma - new drug development strategy: an innovative therapies for children with cancer, European network for cancer research in children and adolescents and international society of paediatric oncology europe neuroblastoma project. *Expet Opin Drug Discov* 2017;12:801–11.
- [6] Lundberg KI, Treis D, Johnsen JL. Neuroblastoma heterogeneity, plasticity, and emerging therapies. *Curr Oncol Rep* 2022;24:1053–62.
- [7] Boeva V, Louis-Brennetot C, Peltier A, Durand S, Pierre-Eugene C, Raynal V, et al. Heterogeneity of neuroblastoma cell identity defined by transcriptional circuitries. *Nat Genet* 2017;49:1408–13.
- [8] Russo M, Siravegna G, Blaszkowsky LS, Corti G, Crisafulli G, Ahronian LG, et al. Tumor heterogeneity and lesion-specific response to targeted therapy in colorectal cancer. *Cancer Discov* 2016;6:147–53.
- [9] Lawson DA, Kessenbrock K, Davis RT, Pervolarakis N, Werb Z, et al. Tumour heterogeneity and metastasis at single-cell resolution. *Nat Cell Biol* 2018;20:1349–60.
- [10] Jindal A, Gupta P, Jayadeva Sengupta D. Discovery of rare cells from voluminous single cell expression data. *Nat Commun* 2018;9:4719.
- [11] Wang X, Duan M, Li J, Ma A, Xin G, Xu D, et al. MarsGT: multi-omics analysis for rare population inference using single-cell graph transformer. *Nat Commun* 2024;15:338.
- [12] Kiselev VY, Andrews TS, Hemberg M. Challenges in unsupervised clustering of single-cell RNA-seq data. *Nat Rev Genet* 2019;20:273–82.
- [13] Cha J, Lee I. Single-cell network biology for resolving cellular heterogeneity in human diseases. *Exp Mol Med* 2020;52:1798–808.
- [14] Chapple RH, Liu X, Natarajan S, Alexander MIM, Kim Y, Patel AG, et al. An integrated single-cell RNA-seq map of human neuroblastoma tumors and preclinical models uncovers divergent mesenchymal-like gene expression programs. *Genome Biol* 2024;25:161.
- [15] Olsen TK, Otte J, Mei S, Embae BT, Kameneva P, Cheng H, et al. Joint single-cell genetic and transcriptomic analysis reveal pre-malignant SCP-like subclones in human neuroblastoma. *Mol Cancer* 2024;23:180.
- [16] Kildisute G, Kholosy WM, Young MD, Roberts K, Elmentait R, van Hooff SR, et al. Tumor to normal single-cell mRNA comparisons reveal a pan-neuroblastoma cancer cell. *Sci Adv* 2021;7:eabd3311.
- [17] Subelj L, Bajec M. Unfolding communities in large complex networks: combining defensive and offensive label propagation for core extraction. *Phys Rev E - Stat Nonlinear Soft Matter Phys* 2011;83:036103.
- [18] Becht E, McInnes L, Healy J, Dutertre CA, Kwok IWH, Ng LG, et al. Dimensionality reduction for visualizing single-cell data using UMAP. *Nat Biotechnol* 2019;37:38–44.
- [19] Stuart T, Butler A, Hoffman P, Hafemeister C, Papalexi E, Mauck WM, et al. Comprehensive integration of single-cell data. *Cell* 2019;177:1888–1902.e21.
- [20] Pugh TJ, Morozova O, Attiyeh EF, Asgharzadeh S, Wei JS, Auclair D, et al. The genetic landscape of high-risk neuroblastoma. *Nat Genet* 2013;45:279–84.
- [21] Liu M, Xia Y, Ding J, Ye B, Zhao E, Choi JH, et al. Transcriptional profiling reveals a common metabolic Program in high-risk human neuroblastoma and mouse neuroblastoma sphere-forming cells. *Cell Rep* 2016;17:609–23.
- [22] Newman AM, Steen CB, Liu CL, Gentles AJ, Chaudhuri AA, Scherer F, et al. Determining cell type abundance and expression from bulk tissues with digital cytometry. *Nat Biotechnol* 2019;37:773–82.
- [23] Kolb H, Kempf K, Martin S. Health effects of coffee: mechanism unraveled? *Nutrients* 2020;12:1842.
- [24] Southgate L, Machado RD, Graf S, Morell NW. Molecular genetic framework underlying pulmonary arterial hypertension. *Nat Rev Cardiol* 2020;17:85–95.
- [25] Keenan TE, Li T, Vallius T, Guerriero JL, Tayob N, Kochupurakkal B, et al. Clinical efficacy and molecular response correlates of the WEE1 inhibitor adavosertib combined with cisplatin in patients with metastatic triple-negative breast cancer. *Clin Cancer Res* 2021;27:983–91.
- [26] Cole KA, Pal S, Kudgus RA, Ijaz H, Liu X, Minard CG, et al. Phase I clinical trial of the Wee1 inhibitor adavosertib (AZD1775) with irinotecan in children with relapsed solid tumors: a cogr phase I consortium report (ADVL1312). *Clin Cancer Res* 2020;26:1213–9.
- [27] Cole KA, Ijaz H, Surrey LF, Santi M, Liu X, Minard CG, et al. Pediatric phase 2 trial of a WEE1 inhibitor, adavosertib (AZD1775), and irinotecan for relapsed neuroblastoma, medulloblastoma, and rhabdomyosarcoma. *Cancer* 2023;129:2245–55.
- [28] Iksen S, Pothongsrisit, Pongrakhananon V. Targeting the PI3K/AKT/mTOR signaling pathway in lung cancer: an update regarding potential drugs and natural products. *Molecules* 2021;26:4100.
- [29] Evan GI, Vousden KH. Proliferation, cell cycle and apoptosis in cancer. *Nature* 2001;411:342–8.
- [30] Tian Y, Almaraz RT, Choi CH, Li QK, Saeui C, Li D, et al. Identification of sialylated glycoproteins from metabolically oligosaccharide engineered pancreatic cells. *Clin Proteom* 2015;12:11.
- [31] McGrath C, Pattabiraman N, Kellogg GE, Lemcke T, Kunick C, Sausville EA, et al. Homology model of the CDK1/cyclin B complex. *J Biomol Struct Dyn* 2005;22:493–502.
- [32] Roering P, Siddiqui A, Heuser VD, Potdar S, Mikkonen P, Oikonen J, et al. Effects of Wee1 inhibitor adavosertib on patient-derived high-grade serous ovarian cancer cells are multiple and independent of homologous recombination status. *Front Oncol* 2022;12:954430.
- [33] Chiang AJ, Li CJ, Tsui KH, Chang C, Chang YI, Chen LW, et al. UBE2C drives human cervical cancer progression and is positively modulated by mTOR. *Biomolecules* 2020;11:37.
- [34] Grizzi F, Di Biccari S, Fiamengo B, Stifter S, Colombo P. Pituitary tumor-transforming gene 1 is expressed in primary ductal breast carcinoma, lymph node infiltration, and distant metastases. *Dis Markers* 2013;35:267–72.
- [35] Moschou PN, Bozhkov PV. Separases: biochemistry and function. *Physiol Plantarum* 2012;145:67–76.
- [36] Huang S, Liao Q, Li L, Xin D. PTTG1 inhibits SMAD3 in prostate cancer cells to promote their proliferation. *Tumour Biol* 2014;35:6265–70.
- [37] Romero-Arenas S, Ruiz R, Vera-Ibanez A, Colomer-Poveda D, Guadalupe-Grau A, Marquez G. Neuromuscular and cardiovascular adaptations in response to high-intensity interval power training. *J Strength Condit Res* 2018;32:130–8.
- [38] Liu G, Zhao J, Pan B, Ma G, Liu L. UBE2C overexpression in melanoma and its essential role in G2/M transition. *J Cancer* 2019;10:2176–84.
- [39] Wang X, Yin L, Yang L, Zheng Y, Liu S, Yang J, et al. Silencing ubiquitin-conjugating enzyme 2C inhibits proliferation and epithelial-mesenchymal transition in pancreatic ductal adenocarcinoma. *FEBS J* 2019;286:4889–909.
- [40] Dai L, Song ZX, Wei DP, Zhang JD, Liang JQ, Wang BB, et al. CDC20 and PTGG1 are important biomarkers and potential therapeutic targets for metastatic prostate cancer. *Adv Ther* 2021;38:2973–89.
- [41] Li C, Wang Y, Wang S, Wu B, Hao J, Fan H, et al. Hepatitis B virus mRNA-mediated miR-122 inhibition upregulates PTTG1-binding protein, which promotes hepatocellular carcinoma tumor growth and cell invasion. *J Virol* 2013;87:2193–205.
- [42] Xiong Z, Li X, Yang Q. PTGG has a dual role of promotion-inhibition in the development of pituitary adenomas. *Protein Pept Lett* 2019;26:800–18.